ELSEVIER

Mechanical Properties of Cement Pastes and Mortars at Early Ages

Evolution with Time and Degree of Hydration

A. Boumiz,* C. Vernet,* and F. Cohen Tenoudji†
**Centre Technique du Groupe Italcementi-Ciments Français, 78931, Guerville Cedex, France; and †Laboratoire Universitaire d'Applications de la Physique, Université Paris 7 (D. Diderot), 2 Place Jussieu, 75005 Paris, France*

To better understand the relations between the hydration reactions and the evolution of the mechanical properties of concrete, we developed an integrated approach. Ultrasonic, calorimetric, and conductometric techniques were applied simultaneously to the same batches of cement pastes and mortars. Young's modulus of elasticity and Poisson's ratio were determined acoustically and studied as functions of time and of degree of hydration. The amount of hydration needed to reach the beginning of set (percolation threshold of solid phase) was determined using our techniques. Although conditioned by the hydration rate, the mechanical behavior is also related to the microstructure evolution. Two main mechanisms have been evidenced in the development of mechanical properties. The first is the connection of cement particles, for which a percolation model is applied. This concept gives good insight of the setting time. The second mechanism corresponds to the filling of capillary pores by the hydrates. The evolutions of elastic properties and compressive strength have been compared. This study provides a new way for assessing the hydration models and for optimization of high performance concrete formulations. ADVANCED CEMENT BASED MATERIALS 1996, 3, 94–106

KEY WORDS: Cement hydration, Cement pastes, Elastic moduli, Mortars, Percolation transition, Setting time, Shear and compressional waves, Ultrasonic velocity and attenuation

The measurement of the ultrasonic compressional wave velocity has been used for a long time to characterize setting and hardening of cementitious systems [1–7]. For example, Raoult et al. [4] measured the velocity of compressional waves in cement pastes for which hardening was controlled by addition of different amounts of $CaCl_2$; they showed that after setting, the compressional velocity measurement can characterize the behavior of different cement paste formulas.

Byfors [5] found a good correlation between the compressional wave velocity and the compression strength for several types of concrete.

Keating, Hannat, and Hibbert [6] showed that just after mixing, the pulse velocity is governed by the fluid phase, because the water content is relatively high, until the time at which the solid phase becomes interconnected. They pointed out that during the first 2 hours of hydration, the compressional wave velocity was influenced by entrapped air, and the presence of air bubbles caused a strong attenuation of compressional waves. Furthermore, for de-aired cement pastes, they observed a small decrease in pulse compressional velocity during the next 2 hours.

Sayers and Dahlin [7] confirmed, as did Keating, that compressional wave propagation at early times was extremely sensitive to the presence of air bubbles. They showed that cement paste containing a sufficiently large number of air bubbles acts as a high-pass filter over the frequency range employed. They explained the early-time decrease in compressional velocity by the increasing tortuosity of the pore space due to the formation of hydration products.

The elastic properties of an isotropic elastic solid are fully described by two independent elastic constants, bulk modulus and shear modulus, for example. Acoustic wave velocities (compressional and shear velocities) are functions of the two elastic constants. Therefore, a compressional wave velocity measurement is not sufficient to determine any elastic modulus of cement pastes and mortars. A simultaneous measurement of shear velocity will fully provide the two elastic constants.

In 1991, Levassort and Cohen Tenoudji [8], in collaboration with the technical center of Italcementi-Ciments Français Group, developed a prototype system for shear and compressional ultrasonic pulse transmission through cement pastes and mortars. The elastic moduli were obtained at early ages.

Address correspondence to: A Boumiz, Université D. Diderot (Paris 7), LUAP 33-43 Zeme etage, 2 Place Jussieu, 75005 Paris, France.
Received November 10, 1994; Accepted October 24, 1995

ISSN 1065-7355/96/$15.00
SSDI 1065-7355(95)00072-0

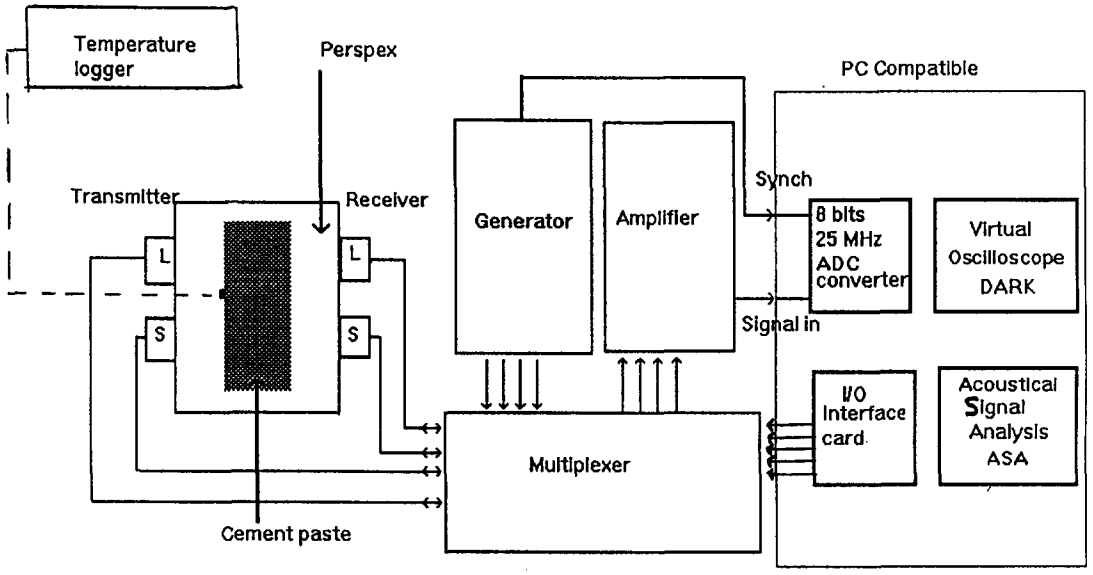

FIGURE 1. Experimental setup.

In 1992, D'Angelo, Plona, and Schwartz [9] examined the propagation of ultrasonic waves in cement paste and showed that shear waves are more sensitive than compressional waves to the solid matrix connectivity. They also noticed a correlation between setting and the beginning of shear wave propagation.

Sayers and Grenfell [10] performed studies similar to those of D'Angelo's group and applied Biot's theory [11] to the evolution of the velocities and attenuation of ultrasonic waves in cement pastes.

Up until now, in acoustics, no systematic study has been performed on the joint evolution of chemical and mechanical properties at early ages. In this work, a series of complementary techniques are used to follow the evolution of the elastic moduli as functions of progress of hydration reactions. First, we present the principles of acoustic measurements and the experimental set-up; then, we describe the chemical behavior, during the different hydration periods, and the chemical measurement techniques giving the time evolution of the hydration rate and electrical conductivity. The elastic parameters are then analyzed as functions of the degree of hydration α to better interpret the mechanical behavior.

Acoustic Measurements

Principles

The measurement of shear and compressional ultrasonic velocities allows the calculation of the elastic coefficients of the material. When the material is isotropic, nondispersive, and the wavelength is large compared to the size of inhomogeneities, the bulk modulus (K), shear modulus (μ), Young's elastic modulus (E), and Poisson's ratio (ν) are given by:

$$K = \rho\left(V_L^2 - \frac{4}{3}V_T^2\right) \tag{1}$$

$$\mu = \rho V_T^2 \tag{2}$$

$$E = 2\mu(1+\nu) \tag{3}$$

$$\nu = \frac{\left(1 - 2\frac{V_T^2}{V_L^2}\right)}{2\left(1 - \frac{V_T^2}{V_L^2}\right)} \tag{4}$$

where V_L and V_T are the velocities of compressional and shear waves and ρ is the cement paste density.

Experiment

We used the transmission of ultrasonic short pulses through the sample. We think that this technique is better than the tone-burst technique, because it allows the separation of the directly transmitted signal from the spurious signals resulting from the multiple reflections on the cell walls. Furthermore, this technique allows a spectral analysis of the received signals, giving directly the attenuation and velocity values as a function of frequency in the same experiment.

EXPERIMENTAL SETUP. The acoustic waves' transmission cell (Figure 1) is made of two parallel perspex walls on which are fixed two pairs of wide-band transducers

TABLE 1. Concrete mortar B35 composition (w/c = 0.524)

Composition	Size Range	Weight (kg)	Density (g/cm³)
Cement	0.1 to 40 μm	340	3.15
Sand	0 to 5 mm	800	2.65
Siliceous filler*	2 to 200 μm	30	2.650
Water		175	1
Melamine based HRWR†		3.4	1.17
Mortar B35			2.253

*Grains of silica for sand granulometric curve correction.
†HRWR = high-range water reducer.

(shear and compressional) of 2.5 cm diameter and 0.5 MHz central frequency. A 3-cm wall thickness was chosen to prevent multiple reflection signals from being superimposed on the useful signal. The sample thickness is adjustable depending on whether cement paste (1 cm) or mortar (4 cm) is observed. For the latter, the size of aggregates requires a larger thickness than in pure cement paste to test a representative volume. The cell is regulated in temperature using a water bath with an accuracy of $\Delta T = \pm 0.02°C$; it is equipped with two platinum Pt 100 sensors for thermal control.

The ultrasonic measurements are performed using short duration electrical pulses (typically 1 μsec) converted to short duration mechanical waves by a piezoelectric transducer. The pulse generator holds 16 multiplexed channels. The range and shape of the emitted pulses (50 to 400 V), the amplification of the received signals, and the emitting/receiving channels are all remote controlled. The signals produced by the receiving transducer are amplified, digitized, averaged, and recorded (Figure 1).

The analog-to-digital conversion is made by an interface card (SONIX STR825) integrated in a personal computer. The card handling, the measurement sequencing, and the pulse generator control are processed using DARK, a laboratory-made software operating as a programmable virtual oscilloscope in the Microsoft Windows® environment. Analysis of received signals is performed using ASA, a software for automatic acoustic signal processing and analysis, that operates in the same environment and was developed at D. Diderot University (LUAP).

TABLE 2. Concrete mortar B60 composition (w/c = 0.387)

Composition	Size Range	Weight (kg)	Density (g/cm³)
Cement	0.1 to 40 μm	425	3.15
Sand	0 to 5 mm	725	2.65
Siliceous filler*	2 to 200 μm	30	2.65
Water		150	1
Melamine based HRWR		14.8	1.17
Mortar B60			2.310

*Grains of silica for sand granulometric curve correction.

TABLE 3. Grey cement paste composition, HPR type (B35)

Composition	% (mass)
SiO_2	19.9
Al_2O_3	4.37
F_2O_3	2.02
TiO_2	0.22
MnO	0.04
CaO	63.10
MgO	3.89
SO_3	3.35
K_2O	0.8
Na_2O	0.08
P_2O_5	0.02
SrO	0.03

PROCEDURES AND SAMPLES. We studied cement pastes and mortars formulated by the Ciments Français Technical Center for a set of building applications according to concrete workability and strength criteria. The mortars called B35 and B60 are the granular size fraction below 5 mm of the corresponding concretes (concrete mortars). Tables 1 and 2 give their compositions with their water/cement mass ratio. The cements used in these two concrete mortars are French-type HPR (fast high performance) grey cements (chemical compositions are given in Tables 3 and 4). In addition, we studied pure pastes of HPR-type white cements, coded PCCB9401 and PCCB9402 (Tables 5 and 6). Table 7 shows the compressive strength development during the first 2 days of the concrete mortar B35 at 25°C and compressive strength ($T = 20°C$) on concrete B35 and B60 at 1, 2, 7, and 28 days. Table 8 gives the following standard tests results for the cements: setting time using the Vicat needle, and compressive strength at 1, 2, 7, and 28 days on 4 × 4 × 16-cm standard mortar prisms.

The concrete mortars were mixed according to the NF EN 196-1 (French standard mixing method). To avoid any entrapped air, the samples were vacuum pumped

TABLE 4. Grey cement paste composition, HPR type (B60)

Composition	% (mass)
SiO_2	20.25
Al_2O_3	4.4
F_2O_3	1.98
TiO_2	0.22
MnO	0.03
CaO	63.26
MgO	3.94
SO_3	3.23
K_2O	0.76
Na_2O	0.13
P_2O_5	0.02
SrO	0.06

TABLE 5. White cement composition (PCCB9401)

Composition	% (mass)
SiO_2	18.1
Al_2O_3	2.06
F_2O_3	0.29
TiO_2	0.08
MnO	0.01
CaO	63.05
MgO	0.54
SO_3	2.39
K_2O	0.69
Na_2O	0.23
P_2O_5	0.02
SrO	0.08

TABLE 6. White cement composition (PCCB9402)

Composition	% (mass)
SiO_2	21.68
Al_2O_3	4.17
F_2O_3	0.29
TiO_2	0.2
MnO	0.01
CaO	66.23
MgO	0.55
SO_3	3.54
K_2O	0.07
Na_2O	0.02
P_2O_5	0.04
SrO	0.14

for 30 minutes. If air bubbles are present in the mix, they modify the values of the elastic coefficient values and the quality of the ultrasonic signals [6,7] and they cause a tremendous attenuation of the compressional waves prior to setting.

EVALUATION OF VELOCITIES AND ELASTIC MODULI. The compressional and shear wave signals are recorded every 10 minutes for 24 hours for cement pastes and for 48 hours for mortars. Waterfall plots of these signals (for increasing hydration time) allow a good overview of the evolution of material properties (Figures 2 and 3). We note that the variation of the transit time is more important for shear waves than for compressional waves. In fact, unlike the compressional waves, the shear waves are not transmitted through water or in the fresh paste before setting. During setting, the fast evolution of the shear waves' transit time is in relation with the connection of the solid particles.

All the cement pastes show similar time evolutions; for example, Figure 4 shows the evolutions of the shear and compressional wave velocities for the white cement paste (PCCB9402). The compressional wave velocity just after mixing is about 1500 m/sec, a value close to the propagation velocity in water. The arrival of shear waves appear at a later time when a continuous path of connected grains is created through the paste. The ultrasonic waves' velocities increase rapidly during setting and more slowly afterwards. From the velocity values and density, we calculate the Young's, shear, and bulk moduli (Figures 5 and 6). These moduli increase strongly at early ages and then increase more slowly when hydration slows down. The Poisson's ratio decreases from about 0.5 (Poisson's ratio value in a fluid) to about 0.2, which is characteristic of a cementitious system.

SPECTRAL EVOLUTION OF ULTRASONIC SIGNALS. Figure 7 shows the evolution of the spectral amplitude of the shear signals at different times of cure. We note an increase in amplitude and a shift of the frequency of the maximum spectral amplitude toward higher frequencies with increasing hydration time.

In fact, at very early ages, the cement paste shows a viscoelastic behavior; it loses energy when it undergoes a deformation, and, therefore, its elastic moduli are complex and depend upon the excitation frequency f. Let us write $G(\omega)$, the shear modulus as function of pulsation $\omega = 2\pi f$

$$G(\omega) = G'(\omega) + j\, G''(\omega) \tag{5}$$

where $G'(\omega)$ is the storage modulus and $G''(\omega)$ is the dissipative modulus. There are many causes of this loss, such as the viscous effect inside the fluid, the diffraction of acoustic waves by heterogeneities, and the fluid movement with respect to the solid matrix (Biot) [11].

In a viscoelastic medium, the phase velocity $V(\omega)$ and the intrinsic attenuation $\alpha(\omega)$ in the material, for a

TABLE 7. Compressive strength evolution of concrete mortar B35 and B60 measured according to European Committee Normalization (CEN) specifications on 4 × 4 × 16-cm prisms

	Compressive Strength (MPa)		
Time	Concrete Mortar B35 (T = 25°C)	Concrete B35 (T = 20°C)	Concrete B60 (T = 20°C)
6 h	0.4		
9 h	4.5		
12 h	9.75		
15 h	16		
18 h	20.5		
21 h	24		
24 h	27	20.8	48.9
27 h	28.75		
33 h	33.5		
39 h	36		
45 h	39		
2 days		30.2	
7 days		40	60.2
28 days		46.7	64.5

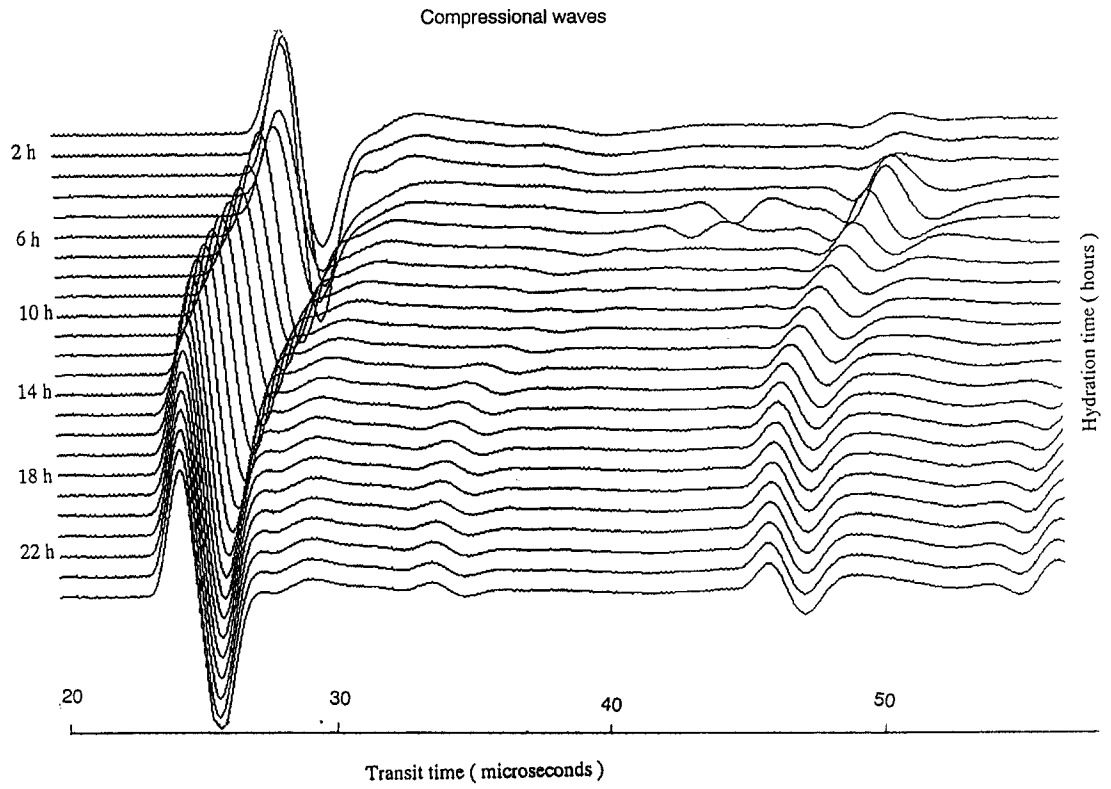

FIGURE 2. Waterfall plot of compressional waves at increasing hydration times (white cement paste PCCB9402, w/c = 0.4, T = 25°C).

monochromatic wave of pulsation ω, are given by (see Bourbié [12])

$$V(\omega) = \sqrt{\frac{2(G'^2(\omega) + G''^2(\omega))}{\rho\left(\sqrt{G'^2(\omega) + G''^2(\omega)} + G'(\omega)\right)}} \tag{6}$$

$$\alpha(\omega) = \omega \sqrt{\frac{\rho}{2}\left[\frac{1}{\sqrt{G'^2(\omega) + G''^2(\omega)}} - \frac{G'(\omega)}{G'^2(\omega) + G''^2(\omega)}\right]}. \tag{7}$$

The attenuation α(ω) is all the more important as $G''(\omega)$ and frequency are high.

Just after mixing, the cement paste is in a viscous elastic state and the imaginary part of the elastic modulus is high; therefore, high frequencies are strongly attenuated. In Figure 8, the spectral amplitudes relative to the amplitude obtained at 12 hours are plotted for three different cure times (3, 6, and 9 hours). The attenuation decreases with cure time and is always greater at high frequencies. The more the material hardens, the more it looses its viscoelastic characteristics, so $G''(\omega)$ decreases. During the whole cure, the medium acts as a low-pass filter on the ultrasonic signals. As G'' decreases, the average frequency of the signal increases with time (Figure 9).

Chemical Behavior

Chemical Measurements

PRINCIPLES. The overall degree of hydration $\alpha(t)$ can be defined by the ratio of the heat released up to time t to the total heat produced when hydration is complete:

$$\alpha(t) = \frac{Q(t)}{Q_\infty}. \tag{8}$$

$Q(t)$ is the result of the heat flow integration, measured in a differential conduction isothermal calorimeter specially designed and calibrated for mortar measurements. Q_∞ is known from hydration of the pure constituents; it is estimated, as a first approximation, as follows:

$$Q_\infty = -(A\ \Delta H_{C_3S} + B\ \Delta H_{C_2S} + C\ \Delta H_{C_3A} + D\ \Delta H_{C_4AF}) \tag{9}$$

where ΔH_{C_3S}, ΔH_{C_2S}, ΔH_{C_3A} and ΔH_{C_4AF} are respectively the hydration enthalpies of the phases. A, B, C, and D are the mineralogical proportions of the respective phases, calculated from the Bogue's formula (or preferably determined from quantitative X-ray diffraction analysis). The enthalpies of the clinker phases can

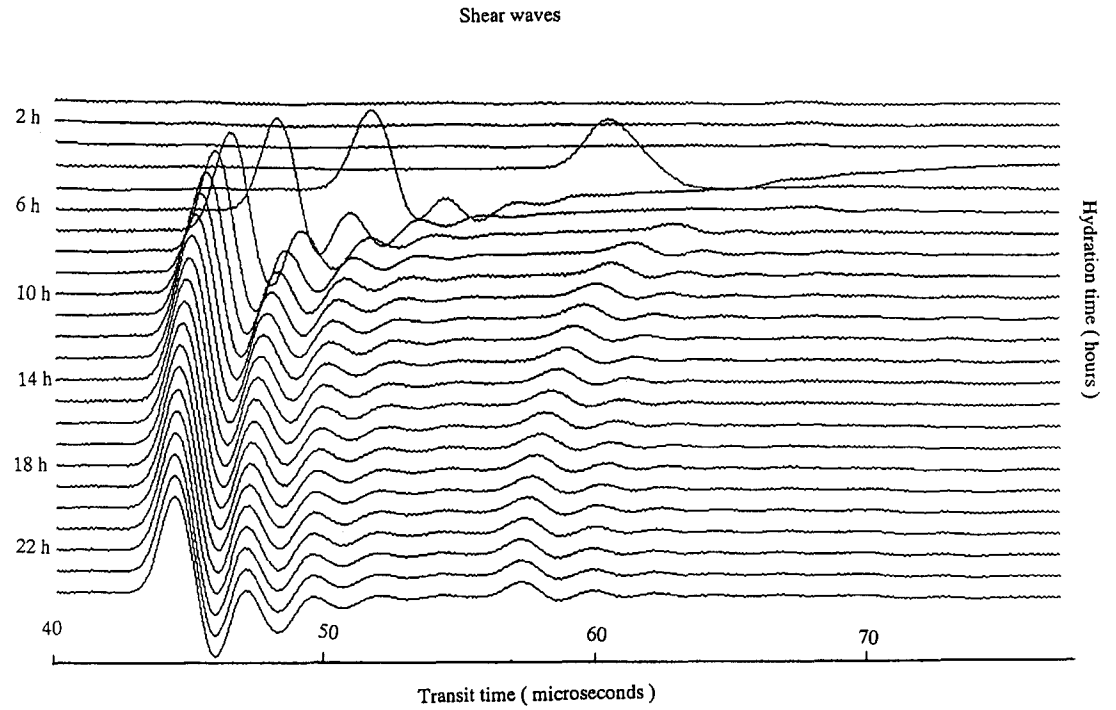

FIGURE 3. Waterfall plot of shear waves at increasing hydration times (white cement paste PCCB9402, w/c = 0.4, T = 25°C).

be slightly different from the tabulated pure phases values. This method of calculation might result in a systematic error in the value of the degree of hydration, Q_∞, being known within the margin of a multiplicative constant. For that reason, comparisons of the degrees of hydration of different sample formulations are more accurate when the same cement is used.

TECHNIQUES. The electrical conductivity during early ages is measured to show the variations in ionic content of the aqueous phase. The cone-shaped cell of the calorimeter is equipped with two annular stainless steel electrodes. The electrical conductance of the paste is measured by applying a 16 kHz sinusoidal voltage to prevent polarization of the electrodes. The cell constant is measured using 0.1 M KCl and 0.01 M KCl solutions. We have verified that there is no variation in cell constant in the range 10–20 kHz.

The integration of the heat rate with time gives the heat of hydration. A temperature probe (Pt 100) is placed inside the paste and another probe is placed on the core periphery. A third probe measures the temperature of the cell regulation fluid coming from the thermoregulated bath. The calorimeter is calibrated using a heating resistor. The temperature data are stored using a Hewlett Packard data logger. The accuracy is about ±0.01°C. Using a differential technique, the base line can be stabilized in the range ±0.01°C/week.

Results

Figure 10 shows the electrical conductivity, the rate of heat evolution, and the heat of hydration as functions of time from mixing. The conductivity maximum corresponds to the end of the induction period and the beginning of portlandite precipitation. During this period, the rate of heat evolution remains low. The acceleration period is marked by a quick increase in rate of heat evolution indicating a renewed hydrates formation. A fast decrease in electrical conductivity can be observed. In mortars and cement pastes, filling pores increases the tortuosity of the porous body. This is a cause of the

TABLE 8. Results of standard tests performed at 20°C on studied cement pastes

Cement Type	w/c	Setting Time (Vicat needle)	Compressive Strength, R_C (MPa)*			
			1 day	2 days	7 days	28 days
Grey cement (B35)	0.5	2 h 50 min	19.4	36.2	54.4	64.8
White cement (PCCB9401)	0.42	1 h 55 min	26.4	41.8	62.3	72.1

*The compressive strength is measured on CEN standard mortars.

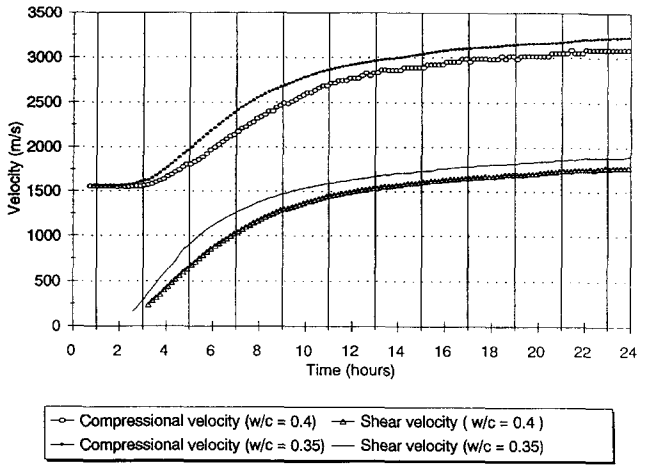

FIGURE 4. Evolution of the ultrasonic velocities in a white cement paste PCCB9402 (w/c = 0.4 and 0.35, T = 25°C).

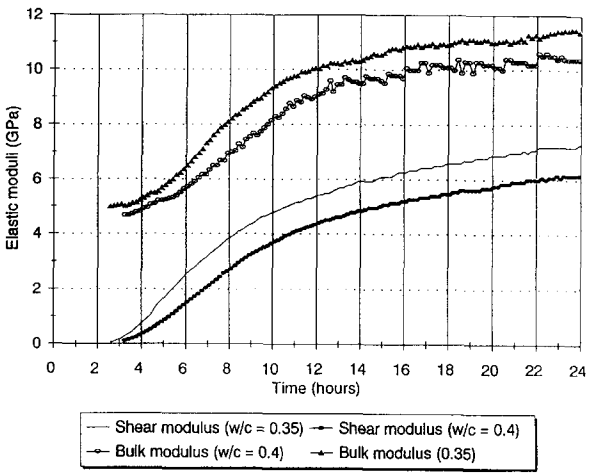

FIGURE 6. Evolution of the bulk modulus and the shear modulus in a white cement paste PCCB9402 (w/c = 0.4 and 0.35, T = 25°C).

decrease in conductivity, added to the well-known ionic concentration drop during this period. In dilute cement suspensions, the electrical conductivity decreases more slowly [13] because the tortuosity remains constant. The gypsum depletion (at about 11 hours in the example Figure 10) is detected by a slope change of the rate of heat evolution and conductivity curves. This is related to ettringite dissolution causing alterations of the microstructure and alkali plus OH ion liberation from the dissolved C_3A during monosulfate formation [13]. Afterwards, the decrease in rate of heat evolution (the slowing down of hydration reactions) is caused by the limitation of water and ionic diffusion through the hydrate layers that have become thicker.

Interpretation

Behavior at Very Early Ages (Percolation)

The hydrates can nucleate and grow both on the surface of the clinker particles and in the porous space. As a result of the chemical bonds created, the solid particles become more and more connected and the material changes from the state of a suspension of clinker particles of irregular shape to the state of a porous elastic solid that has well-defined elastic moduli.

The hydrates around the cement grains cause the formation first of small isolated clusters then of bigger clusters, with increasing degrees of connectivity. The interconnected solid network continues to develop until it spreads throughout the material. At this critical time, the shear wave may propagate throughout the material.

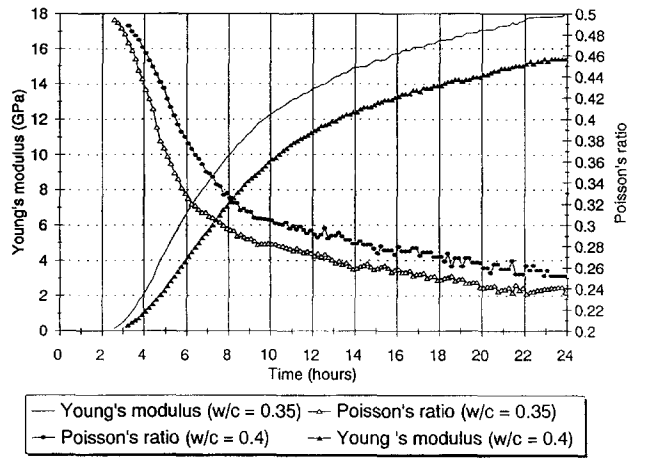

FIGURE 5. Evolution of Young's modulus and Poisson's ratio in a white cement paste PCCB9402 (w/c = 0.4 and 0.35, T = 25°C).

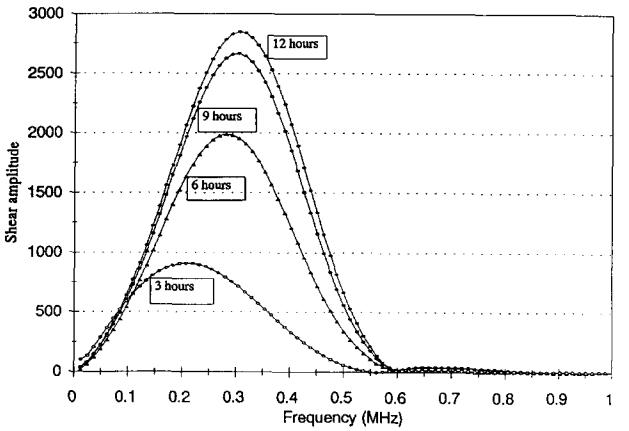

FIGURE 7. Comparison of shear waves spectra at increasing hydration times (white cement paste PCCB9402, w/c = 0.4, T = 25°C).

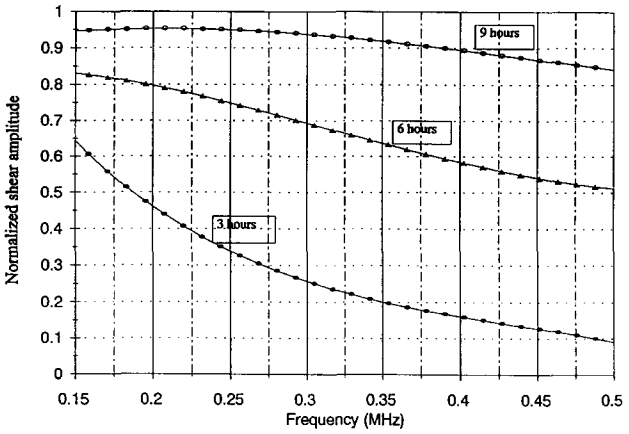

FIGURE 8. Comparison of normalized shear waves spectra at increasing hydration times (white cement paste PCCB9402, w/c = 0.4, T = 25°C).

This transition from a suspension of clinker particles in water to an interconnected solid phase can be considered as a percolation transition [14,15]. The fraction of mechanical contact (p_c) necessary to allow this transition will be called the percolation threshold.

Beyond the percolation threshold, the shear modulus μ increases according to a power law [16,17]

$$\mu = \mu_0 (p - p_c)^{\nu} \tag{10}$$

where p is the fraction of created bonds, ν is the percolation critical exponent, μ_0 is a constant.

Assuming, as Gauthier et al. [18] did, that the number of contacts between the clinker particles increases as a power law function of the time t, in the neighbourhood of the critical time t_c, the shear modulus is obtained:

$$\mu = \mu_0' (t - t_c)^{\nu'} \tag{11}$$

where μ_0' and ν' are constants.

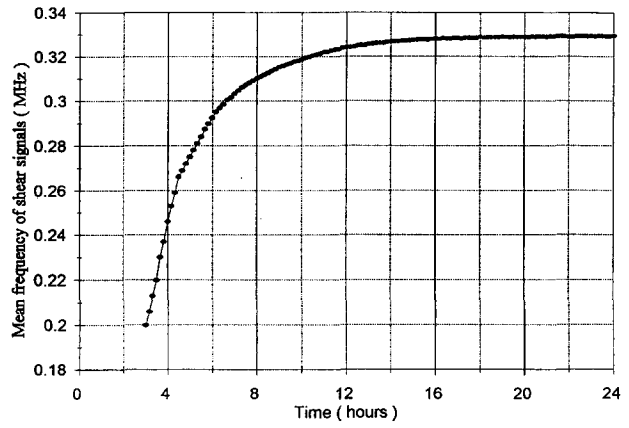

FIGURE 9. Evolution of mean frequency of shear signals (white cement paste PCCB9402, w/c = 0.4, T = 25°C).

Figures 11 and 12 show, respectively, the compressional wave velocities and the shear wave velocities as functions of time for white cement pastes (PCCB9401) prepared with w/c ratios of 0.34, 0.4, and 0.5. Just after mixing, the velocity of the compressional wave is about 1500 m/sec and remains practically constant during the dormant period. We note also a higher compressional velocity for a higher solid concentration (Figure 11) in agreement with the results of Johnson and Plona [19].

For the first few hours after mixing, the compressional wave velocity decreases slightly, reaches a minimum, and then increases. This can be interpreted in the following way: The first created hydrates allow the formation of the first clusters of connected clinker particles, contributing to the increase in medium tortuosity. This leads to the diminution of the compressional velocity [11] down to the point where wave propagation no longer occurs in water but occurs in the connected grains.

The exponent ν' can be determined from the experimental results by fitting it to a straight line (Figure 13a) with the equation:

$$\mathrm{Ln}(\mu) = \mathrm{Ln}(\mu_0) + \nu' \,\mathrm{Ln}(t - t_c). \tag{12}$$

t_c is obtained by choosing from the possible values the one that gives the maximum correlation coefficient of the linear fit (Figure 13b). The critical exponent is then the slope of the regression line obtained for that t_c.

Table 9 presents the percolation time and critical exponents ν' of white cement pastes of different compositions. The time of percolation t_c is located between the beginning of the increase in compressional velocity and the first detection of shear waves. We think that, at the percolation threshold, the cement paste develops a nonzero shear modulus, but the strong attenuation of the viscoplastic medium does not allow the detection of these very first shear waves.

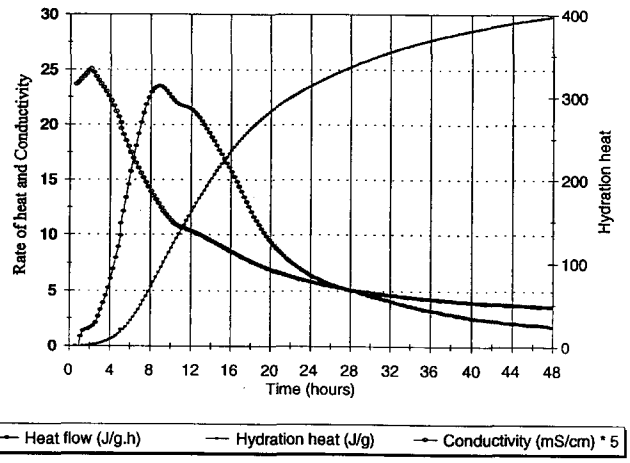

FIGURE 10. Evolutions of the electrical conductivity, rate of heat evolution, and hydration heat in concrete mortar B35 (T = 25°C).

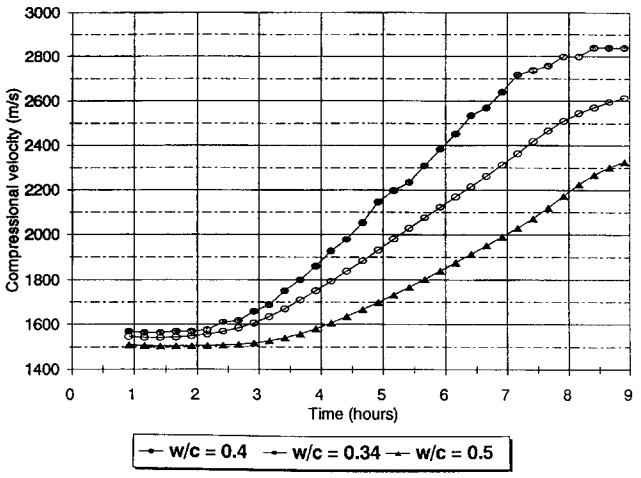

FIGURE 11. Variation of compressional wave velocity with the w/c ratio at very early ages (white cement paste PCCB9401, T = 25°C).

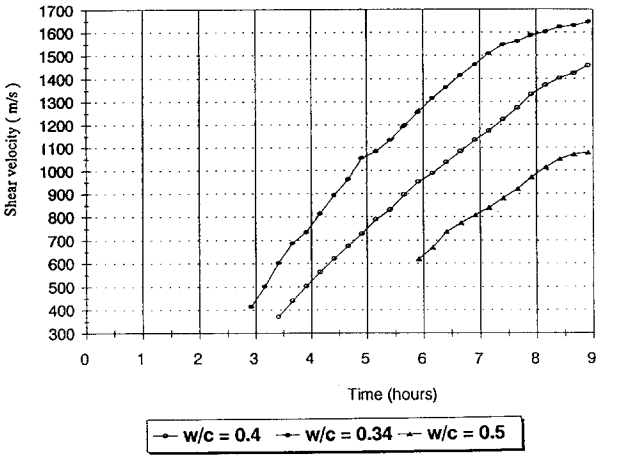

FIGURE 12. Variation of shear wave velocity with the w/c ratio at very early ages (white cement paste PCCB9401, T = 25°C).

The percolation threshold occurs sooner for a lower w/c ratio (Table 9). When the w/c ratio is decreased, the cement particles are closer, and setting occurs sooner.

The differences between the exponents v' in Table 9 do not seem significant. The critical times are very close to the time of first increase in compressional wave velocity. We can conclude that the percolation threshold gives a physical meaning to the setting time that can be evaluated using our technique.

We have determined the critical degree of hydration of white cement PCCB9402 corresponding to the mechanical percolation threshold. We found α_c = 0.015 for w/c = 0.35 and α_c = 0.021 for w/c = 0.4.

The degree of hydration at the percolation threshold varies with the w/c ratio in accordance with works about simulations developed in 1993 by Bentz et al. [20]. They created cellular automaton algorithms to model the microstructure evolution related to the creation of hydrates by chemical reactions. They determined the degree of hydration at the mechanical beginning of set (percolation threshold of the solid phase). For C_3S paste prepared with 0.35 w/c ratio, they found a degree of hydration at percolation threshold to be 0.018, close to our experimental value (α_c = 0.015) of white cement paste prepared with the same w/c ratio.

Our results are slightly smaller than those found by Chen and Odler [21] determined using the Vicat probe (ASTM C191).

Relation Between the Chemical and Mechanical Evolutions

TIME EVOLUTION. We have studied several cement pastes and concrete mortars. Figure 14 presents, as an example, the results on concrete mortar (B35 type). After the electrical conductivity maximum at t = 2 hours,

TABLE 9. Percolation times and exponents v' of white cement pastes

Cement Paste	Beginning of the Increase in Compressional Velocity	Percolation Times t_c	Time of First Detection of Shear Wave	Exponent v'
PCCB9402 w/c = 0.4 T = 25°C	145 min	160 min	195 min	2.15
PCCB9402 w/c = 0.35 T = 25°C	105 min	120 min	155 min	2.03
PCCB9401 w/c = 0.4 T = 25°C	105 min	135 min	210 min	1.92
PCCB9401 w/c = 0.34 T = 23°C	90 min	125 min	165 min	2.13

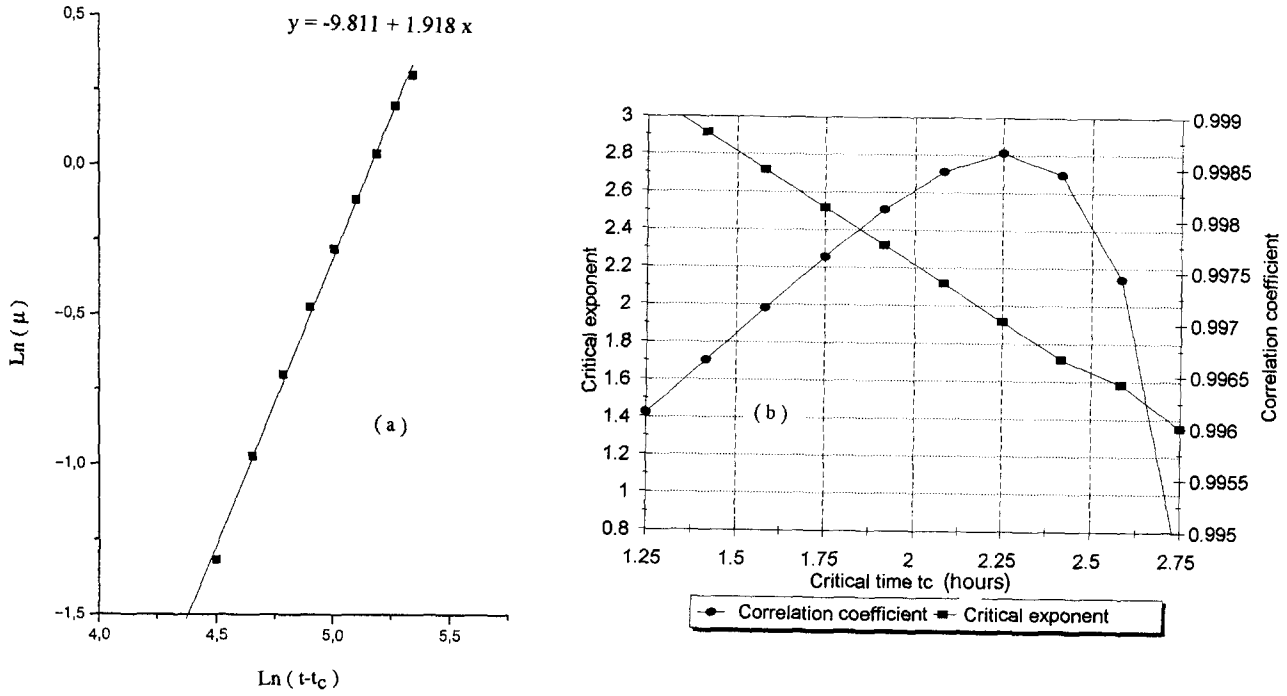

FIGURE 13. Determination of the exponent ν' (white cement paste PCCB9401, w/c = 0.4). (a) Linear regression; (b) critical exponent ν' and correlation coefficient.

which indicates the end of the induction period, the acceleration period begins, noted by a fast increase in thermal flow followed by a strong increase in compressional velocity and the detection of shear wave arrivals. A rapid increase in Young's modulus and a decrease in Poisson's ratio also occur (Figure 15). It can be seen that these variations appear after the beginning of the increase in thermal flow. As a matter of fact, it is necessary to create enough hydrates to reach the percolation threshold.

The variation of Young's modulus and Poisson's ratio with respect to the degree of hydration can be analyzed in three evolution regimes:

- Grain connection regime. At the end of the induction period, portlandite crystals begin to grow. This results in an acceleration of the hydration reactions, forming both portlandite and calcium silicate hydrate (CSH). This reaction first concerns the surface of the clinker grains and gives rise to pro-

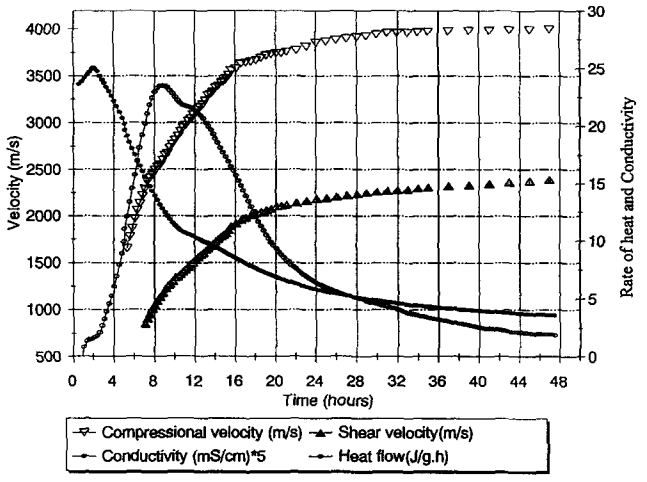

FIGURE 14. Development of ultrasonic velocities compared with chemical evolution in mortar B35 (T = 25°C).

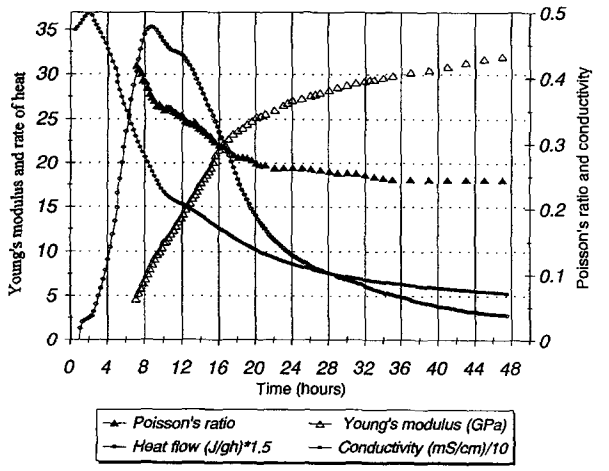

FIGURE 15. Development of elastic properties compared with chemical evolution in mortar B35 (T = 25°C).

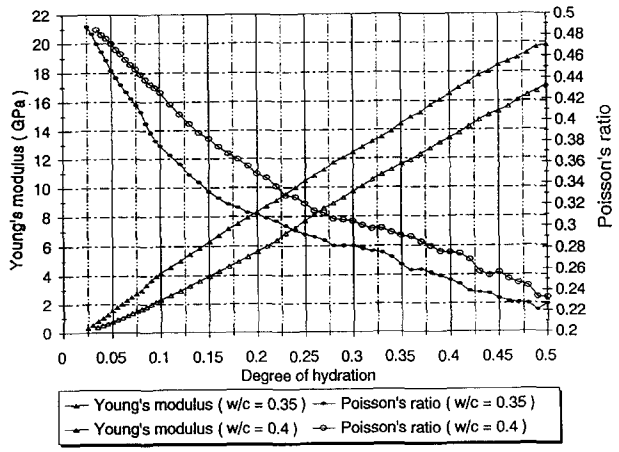

FIGURE 16. Young's modulus and Poisson's ratio as function of the degree of hydration for white cement pastes PCCB9402 (T = 25°C).

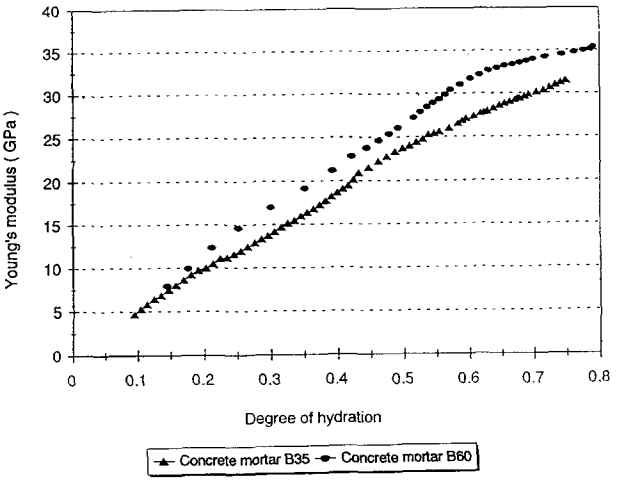

FIGURE 17. Comparison of the evolution of Young's moduli with the degree of hydration for mortars B35 and B60.

gressive connection between grains. During this connection period, there is a fast decrease in Poisson's ratio. The degree of connection, evaluated from the variation of the shear modulus, increases with time according to a power law for which we determined the exponent for white cement pastes (Table 9). The period of rapid increase in elastic moduli matches the hydration acceleration period (Figure 15).

- Transitional regime (grain connection and pore filling). In this regime, the reactions are controlled by diffusion of water and ions through the hydrate layers, the thickness of which has increased. The thermal flow decreases. This period corresponds to a slower evolution of Young's modulus and slower reduction of Poisson's ratio (Figure 15). We think that pore filling occurs inside the first clusters of connected grains before the total connection of grains.
- Pore-filling regime. The total connection between the grains is followed by a third evolution regime, during which hydration only fills the capillary pores. The relative increase in Young's modulus due to the formation of a given amount of hydrates during this pore-filling phase is smaller than that obtained during the grain connection period.

EVOLUTION WITH DEGREE OF HYDRATION (α). The issue about the relation between compressive strength and degree of hydration has been previously discussed [22,23]. Our motivation was to know the influence of the volume of hydrates on the development of the mechanical strength of the material. Among the parameters that have an impact on the relation between R_c and α, the curing temperature, cement composition, and the w/c ratio can be quoted. The w/c ratio strongly affects the development of compressive strength and Young's modulus. When the w/c ratio decreases, the cement particles are closer, and the amount of hydrates required to fill the porous space is small.

Figure 16 shows Young's modulus and Poisson's ratio as a function of the degree of hydration of the white cement pastes prepared with 0.35 and 0.4 w/c ratio. At the same degree of hydration, the Young's modulus is higher as the w/c ratio is small. On the contrary, the Poisson's ratio is smaller as the w/c ratio is small. This can be easily understood by the fact that at the same degree of hydration, the cement paste prepared with higher w/c ratio contains relatively more water.

Féret proposed a formula giving the compressive strength of mortars [24] as a function of the initial porosity ϵ_i

$$R_c(\alpha) = R_c^*(\alpha)(1 - \varepsilon_i)^2 \tag{13}$$

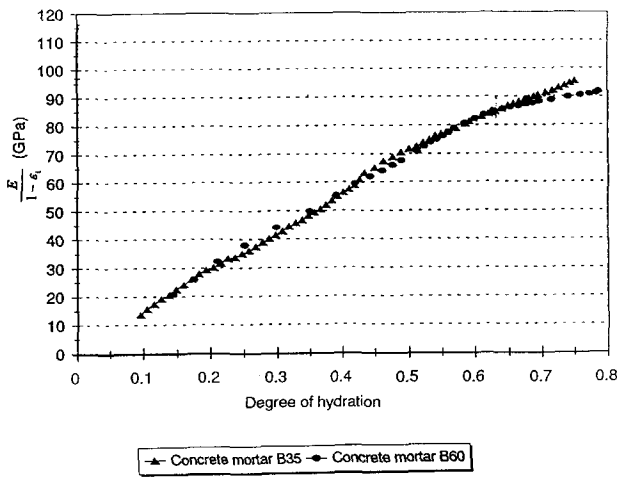

FIGURE 18. Young's modulus corrected of the influence of the initial porosity versus degree of hydration for mortars B35 and B60.

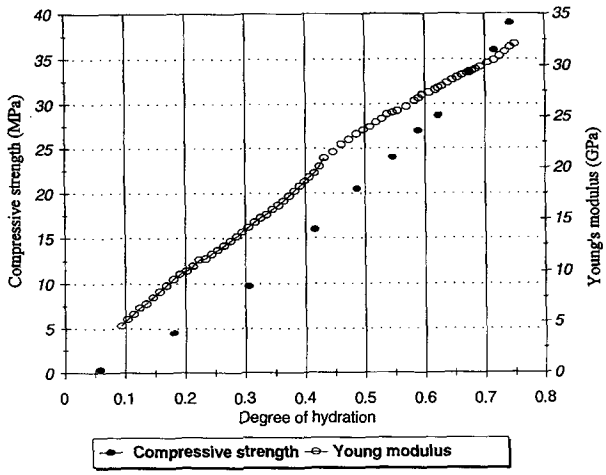

FIGURE 19. Compressive strength and Young's modulus as functions of degree of hydration in mortar B35 (T = 25°C).

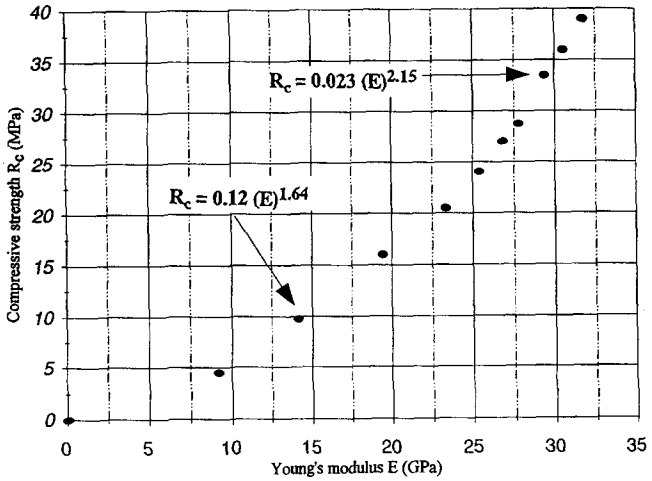

FIGURE 21. Relation between compressive strength and Young's modulus for mortar B35 (T = 25°C).

where

$$\epsilon_i = \frac{V_w + V_a}{V_c + V_w + V_a}. \tag{14}$$

V_w, V_c, and V_a are the initial volume fraction of water, cement, and air, and R_c^* (α) is the compressive strength corrected of the influence of the initial porosity, allowing the comparison of results obtained on samples of different w/c ratios. R_c^* (α) depends only on the degree of hydration α.

For the B35 and B60 mortars, we have tested a relation analog to Féret's formula, giving the Young's modulus

$$E\ (\alpha) = E^*\ (\alpha)\ (1 - \epsilon_i) \tag{15}$$

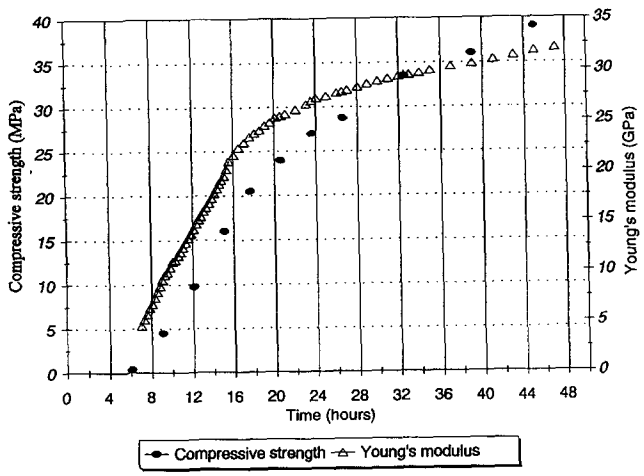

FIGURE 20. Compressive strength and Young's modulus as functions of time in mortar B35 (T = 25°C).

where E^* (α) is the Young's modulus corrected of the influence of the initial porosity of the material.

We have taken an exponent of one instead of two for the term in parenthesis; as we will see in the next paragraph, the later age compressive strength varies approximately as the square of the Young's modulus.

Figure 17 shows the Young's modulus evolution of mortar B35 and B60 as a function of the degree of hydration. Figure 18 shows the ratio $(E)/(1 - \epsilon_i)$ as a function of the degree of hydration for these two mortars in order to obtain values corrected for initial porosity. We have taken V_a = 0, because we have deaerated the samples before the experiment. We note that the curves for the two mortars are well superimposed in agreement with eq 15.

Figure 19 shows the curves of Young's modulus and compressive strength as functions of the degree of hydration. The compressive strength R_c measured on 4 × 4 × 16 prisms increases slowly during the grain connection period and much faster during the pore-filling regime. During the connection period, the solid is viscoplastic and R_c increases slowly with degree of hydration. The strength of the medium develops during the second phase by pore filling.

Correlation Between Young's Modulus and Compressive Strength Values

Taking into account the heterogeneous nature of the mortar, the theoretical relationship between Young's modulus and compressive strength is presumably complex (Figure 20). For that reason, we have only tried to establish an empirical relationship. Figure 21 shows a good correlation between Young's modulus and compressive strength. For the mortar B35 studied here, we have observed two behaviors. During the connection

period ($\alpha < 0.4$, $t < 16$ h for B35 mortars), we found the following power law relating R_c (in MPa) to E (in GPa):

$$R_c = 0.12\ (E)^{1.64}. \quad (16)$$

For the pore filling period ($\alpha > 0.4$, $t > 16$ h for B35 mortar), we found

$$R_c = 0.023\ (E)^{2.15}. \quad (17)$$

This relation is in good agreement with the empirical laws previously established for concretes at ages between 7 and 28 days [25] that state that compressive strength varies as the square of static Young's modulus.

In the full α range, we find:

$$R_c = 0.102\ (E)^{1.7}. \quad (18)$$

We may foresee the existence of a general law for the first regime (grain connection); but its establishment requires very sensitive measurements of R_c. A general law should be a function of the degree of hydration α.

Conclusion

We have presented a combined experimental approach of the study of setting and hardening of cement pastes and mortars. Joint measurements of ultrasonic velocities, electrical conductivity, and heat flow have been performed.

Elastic moduli have been obtained from measured compressional and shear velocities values. The early increase elastic moduli were analyzed using a percolation approach, and the critical times corresponding to the percolation threshold were established. The percolation threshold occurring when an "infinite" cluster of connected grains has formed throughout the material gives a precise physical meaning of the beginning of set.

The degree of hydration given by calorimetry measurements allows us to compare the evolution of the elastic moduli with the progress of the chemical reactions. Two main evolution regimes were identified. The study of the evolution of Young's modulus and compressive strength, as functions of the degree of hydration, shows the sensitivity of the elastic moduli to the connection between particles, whereas strength is more sensitive to the pore filling.

The Féret's initial porosity factor can be used as a rough model of the influence of the water content in mortars on Young's modulus variations.

Another study is in progress where this integrated approach is applied in experiments performed at different temperatures. The results might be used to assess the activation energy concept for the elastic coefficients and to compare the obtained values with the activation energies for chemical reactions.

Acknowledgment

The authors would like to thank J.F. Mourey who realized electronics of the multiplexed pulser receiver.

References

1. Kaplan, M.F. *ACI J.* **1960,** 853–857.
2. Mayfield, B.; Bettison, M. *Concrete* **1974,** 36–38.
3. Elvery, R.H.; Ibrahim, L.A.M. *Mag. Concr. Res.* **1976,** *28,* 181–190.
4. Raoult, F.; Le Bot, J.; Baron, A. *Revue des Matériaux de Construction* **1976,** 698.
5. Byfors, J. *Swedish Cem. Concr. Res. Inst.* **1980,** Fo 3, 80, 344.
6. Keating, J.; Hannat, D.H.; Hibbert, A.P. *Cem. Concr. Res.* **1989,** *19,* 715–726.
7. Sayers, C.M.; Dahlin, A. *Adv. Cem. Based Mater.* **1993,** *1,* 12–21.
8. Levassort, F.; Cohen Tenoudji, F. In *Rapport de D.E.A. d'Acoustique Physique, Université PARIS 7,* **1991.**
9. D'Angelo, R.; Plona, T.J.; Schwartz, L.M. *SPE Prod. Eng.* **1992.**
10. Sayers, C.M.; Grenfell, R.L. *Acoustics* **1993,** *31,* 147–153.
11. Biot, M.A. *J. Acoust. Am.* **1956,** *28,* 168–191.
12. Bourbié, T.; Coussy, O.; Zinszner, B. *Acoustics of Porous Media.* Editions TECHNIP: Paris, **1987.**
13. Vernet, C. *VII Symp. Int. chim. des ciments Paris,* **1980.**
14. Acker, P. *Comportement Mécanique du Béton,* rapport de recherche LCPC, Paris, **1988;** 152.
15. Bentz, D.P.; Garboczi, E. *Cem. Concr. Res.* **1991,** *21,* 325–344.
16. De Gennes, P.G. *J. Physique Lett.* **1976,** *37,* L1–L2.
17. Stauffer, D. *Introduction to Percolation Theory.* Taylor and Francis: London, **1985.**
18. Gauthier, B.; Guyon, E. *C.R. Acad. Sc. Paris* **1980,** t. 290, série B, 465–467.
19. Johnson, D.L.; Plona, T.J.J. *Acoust. Soc. Am.* **1982,** *72,* 556–565.
20. Bentz, D.P.; Coveny, P.V.; Garboczi, E.; Kleyn, M.F.; Stutzman, P.E. *Modelling Simul. Mater. Sci. Eng.* **1994,** *2,* 783–808.
21. Chen, Y.; Odler, I. *Cem. Concr. Res.* **1992,** *22,* 1130–1140.
22. Taplin, J.M. *Austr. J. Appl. Sci.* **1959,** *10,* 329–345.
23. Lawrance, F.V.; Young, J.V.; Berger, R.L. *Cem. Concr. Res.* **1977,** *7,* 369–378.
24. Féret, R. *Ann. Ponts Chaussées* **1892,** 2^e semestre, 5–161.
25. Klink, S.A. *Cem. Concr. Res.* **1992,** *22,* 761–768.